

GRAIN SIZE AND SEISMIC ANALYSIS OF IODP
EXPEDITION 333, SITE C0018 AND THE PINK
VOLCANIC ASH HORIZON, NANKAI TROUGH,
OFFSHORE JAPAN

Research Thesis

Submitted in partial fulfillment of the requirements for graduation

With Research Distinction in Earth Sciences in the

undergraduate colleges of

The Ohio State University


By

Tyler J. Rohan

The Ohio State University

2016

Approved by

A handwritten signature in blue ink, consisting of a large, stylized 'D' followed by a series of loops and a long horizontal stroke extending to the right.

Dr. Derek E. Sawyer, Advisor
School of Earth Sciences

TABLE OF CONTENTS

Abstract.....	ii
Acknowledgements.....	iii
List of Figures.....	iv
List of Tables.....	v
Introduction.....	1
Geologic Setting.....	6
Structural Evolution.....	6
Past Tectonic Activity.....	7
Methods	
Sampling Methods (Coring/Seismic Acquisition).....	9
Hydrometer Analysis.....	9
Mapping in Kingdom.....	14
Data interpretation.....	15
Results	
Grain Size Distribution across the Mass Transport Deposit....	17
Pink Volcanic Ash Horizon.....	19
Discussion	
Variation of Grain Size in Grain Size Analyses.....	22
Potential Causes for Destabilizing the Sea Floor.....	23
Role of the Volcanic Ash in Mobilizing Landslides.....	24
Conclusions.....	27
Suggestions for Future Research.....	28
References Cited.....	29
Appendix.....	32

ABSTRACT

A two part investigation of a mass transport deposit (MTD) in the Nankai Trough, offshore Japan was conducted to learn more about the dynamic behavior of submarine landslides. Hydrometer analysis of 50 sediment samples from the Integrated Ocean Drilling Program (IODP) Expedition 333, Site C0018 was completed with the objective to determine the grain size distribution within a prominent mass transport deposit (MTD-B). Core samples were collected from 90.17 to 191.17 meters below the seafloor (mbsf) with approximately 1 sample per 1 meter collected inside MTD-B. MTD-B was also cored at Site C0021, IODP Expedition 338 providing a valuable opportunity to study a single MTD from two different locations. With the aid of seismic data it was confirmed that both Site C0018 and Site C0021 cored MTD-B. The grain size analysis indicates two major lithologies: clayey silt (78% of samples) and silty clay (15% of samples). The grain size results acquired from Site C0018 were very similar to Site C0021. Both data sets showed a pattern of fining upward inside of the MTD. The grain size analysis of Site C0018 also revealed a defining volcanic ash layer that underlies MTD-B. This observation motivated the second part of this investigation.

This second part of this investigation utilized 3D seismic data to examine the discovered volcanic ash layer. This was done with the objective to determine its role in the mobilization of MTD-B. Through examination of the seismic data it can be seen that the ash layer is displaced by MTD-B before reaching Site C0021. With the discovery of the volcanic ash layer underlying MTD-B it became important to determine the volcanic ash's role in not only in the mobilization of MTD-B, but also in the mobilization of other landslides throughout the Nankai Trough region. With 3D seismic data the volcanic ash horizon was able to be mapped throughout the Nankai Trough seismic survey area. With the horizon mapped it was possible to locate another landslide that is positioned on-top of the same volcanic ash layer, exemplifying how the discovered ash layer may have been a weak layer allowing submarine landslides to mobilize throughout the region.

ACKNOWLEDGEMENTS

The first person I would like to thank is Dr. Derek Sawyer who took me on as an inexperienced researcher and gave me the opportunity to work in his lab. The knowledge and experience I have gained from working with Dr. Sawyer and his graduate students have helped me grow into the geologist I am today. Without their help and guidance, I would not be preparing to defend my thesis as an undergraduate. I would also like to thank my major advisor Dr. Anne Carey who has guided and supported me throughout my academic career at the Ohio State University even when I missed a step or two. I need to thank Dr. Carey and Dr. Christena Cox for giving me the opportunity to become a teaching assistant and use the knowledge I had gained through my major classes to teach others. I need to thank Dr. Krissek whose interesting classes and lectures helped both peaked and affirm my interest in marine science.

I would like to acknowledge the Shell Exploration and Production Company for providing the funding I received during the Shell Undergraduate Research Experience where I first began my thesis research. I would like to acknowledge the International Ocean Discovery Program, specifically expeditions 333 and 338 for collecting samples and data crucial to my thesis. I would like to thank Joshua DeVore for his help and guidance when conducting grain size analysis experiments as well as Zach Moore whose graduate thesis helped guide me through my own research.

I would like to acknowledge my fellow Earth Science classmates who were with me through late night study sessions in Mendenhall Laboratory and long hours in the field during field camp. To my family and friends whose support and guidance continues to help me achieve my scholastic goals; thank you.

LIST OF FIGURES

1.	Bathymetric map and Seismic Profile.....	3
2.	Detailed Surface Morphology.....	4
3.	Seismic Line A-A' with Lithostratigraphic Columns.....	5
4.	Map of the NanTroSEIZE region.....	6
5.	Model for the Development of the Nankai Accretionary Prism.....	7
6.	Map of Potential Seismic Intensity in Japan.....	8
7.	Example Hydrometer Sheet.....	12
8.	Particle Size Distribution Plot.....	13
9.	Shepard Ternary Plot.....	14
10.	Seismic Data through Well Sites.....	15
11.	Reproducibility Test.....	16
12.	Ternary Plot of combined C0018 and C0021 Grain Size Data.....	17
13.	Plot of Particle Size Distribution with LWD Logs from Site C0018.....	18
14.	Particle Size and LWD Plots from Site C0021.....	19
15.	Seismic Data of MTD-B Cutting Pink Volcanic Ash.....	20
16.	3D Model of Pink Volcanic Ash and MTD Deposits.....	21
17.	Model of Depositional History for MTD-B.....	24
18.	Smear Slide Photo of Pink Volcanic Ash.....	25
19.	Seismic Data of Surficial Landslide.....	26

LIST OF TABLES

1.	List of Variables.....	32
2.	Table of Final Grain Size Analysis Data.....	33

INTRODUCTION

The focus of this study is on the examination of a submarine landslide deposit, otherwise called a mass transport deposit (MTD), through both seismic and grain size analysis. A submarine landslide can occur when physical conditions change causing the sea bed to fail and slide downslope. Submarine landslides are among the largest sedimentary transport processes on Earth and can transport sediment from continental slopes to the deep ocean (Masson et al. 2006). There is evidence that the largest submarine landslides can occur on slopes with only 1° degree dips. Submarine landslides are widespread on submarine slopes and can often compose 50% of the stratigraphic record on continental margins (Sawyer et al. 2012). Submarine landslide may be two to three orders of magnitude larger than any terrestrial landslide (Hampton et al. 1996). These landslides have the ability to transport thousands of km³ of sediment downslope. For example a well-known submarine landslide, the Storegga Slide that occurred off the Norwegian Coast involved 3000 km³ of sediment. This massive submarine landslide created an enormous tsunami in the North Atlantic Ocean, affecting approximately 9500 km² of the Norwegian slope and basin and had a run out distance of approximately 800 km (Haflidason et al. 2004).

It is important to study submarine landslides because of the hazards they can pose to both society and industry. The hazardous impact of submarine landslides ranges from the generation of large tsunami to the creation of turbidity currents that disturb biological seafloor communities. The devastating effects on society from a large scale submarine landslide are exemplified through the events which occurred on July 17, 1998 in Papua New Guinea when a landslide created waves rising up to 15 meters high killing an estimated 2,200 people (Moore et al. 2014). From an industrial aspect, submarine landslides can rupture pipelines and damage offshore drilling platforms, which are multi-billion dollar infrastructures.

Two important factors in defining the post-failure behavior of any mass transport deposit are grain size and pre-failure water content. A better

understanding of the dynamic behavior of submarine landslides can help inform others of the security of a certain region and of potential actions to undertake at the seafloor to mitigate the issue. For this reason, analysis of high-quality physical and mechanical data of marine sediments from submarine landslide deposits, both *in-situ* and in the laboratory, is a high priority for gaining a better perspective on both the performance evaluation of submarine slopes and smaller scale physical processes or properties that influence shear failure of marine sediments (Yamada et al. 2012).

This study focuses on a prominent landslide deposit in the Nankai Trough, offshore Japan (Figure 1). Japan is particularly susceptible to marine geohazards such as submarine landslides. There were two primary aims to this thesis work: (1) conduct a detailed downhole grain size analysis of a prominent landslide deposit from IODP Site C0018, and (2) map both the landslide deposit MTD-B and pink volcanic ash layer that underlies it in three dimensions using reflection seismic data. Such data will provide valuable insight into the dynamic behavior of landslides along this active margin. All samples and 3D seismic data have been made available in Dr. Sawyer's lab for this study. Due to the fine-grained nature of the sediments, particle size analysis has been conducted using the standard hydrometer method. The hydrometer method was used to determine mass fraction of clay size, silt size, and sand size particles for each sample. Lithology was classified according to the Shepard (1954) classification. The data collected have been used to 1) document vertical variation in grain size distribution of the large mass transport deposit, 2) enhance the understanding of the depositional history of Site C0018, and 3) understand the three-dimensional structure and morphology of the landslide deposit. Study of grain size distribution within this mass transport deposit will provide insight toward a better understanding of the flow behavior within mass flow during transport.

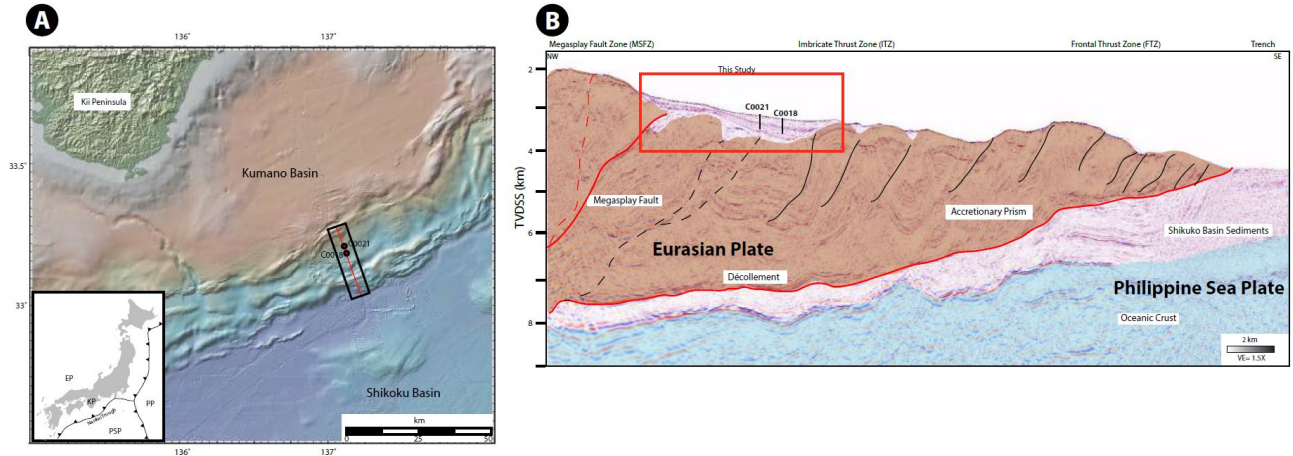


Figure 1: Geologic setting for slope basin sediments in Nankai. (A) Bathymetric map showing location of IODP sites C0021 and C0018. Modified from (Moore and Sawyer, 2014) Black rectangles show location three-dimensional seismic volume and red line indicates the location of the seismic line transect in Figure 3. In set map shows the tectonic setting and plate configuration of Nankai Trough. (B) Seismic profile indicating the major tectonic regions within the accretionary prism. The Slope basin studied here lies seaward of the megasplay fault zone. Modified from (Strasser et al. 2011).

Particle size distribution is a fundamental property that plays a key role in the dynamic behavior of submarine landslides (Sawyer et al. 2012). The flow behavior of submarine landslides is important to understand because one of the key factors which controls the size of a landslide-induced tsunami is initial slide motion. Rapid acceleration is an important variable which has been associated with the creation of slide-generated tsunami (Alves et al. 2014). The high cost of deep sea coring makes this an extremely rare opportunity to acquire detailed information on a single landslide. The data generated within this study complement results which had been collected from Site C0021 (Moore and Sawyer 2014). Analysis of a larger sample size from a different location of the same mass transport deposit will decrease the possible random error in the data set.

The potential for geohazards in the Nankai Trough region has attracted heavy interest from IODP with a multi-expedition science program called the NanTroSEIZE project. This program has been run from 2007 to present and has so far consisted of 11 different IODP expeditions. The NanTroSEIZE project was broken up into 3 Stages with Stage 1 consisting of expeditions 314, 315, and 316 which carried out a unified drilling program on eight selected sites on the frontal

thrust region, the midslope Megasplay fault region, and the Kumano forearc basin (Moore et al. 2014). Stage 2 of the NanTroSEIZE included 4 IODP expeditions 319, 322, 332 and 333 (Henry et al 2012). The goal of Stage 2 was to expand on the knowledge gained in Stage 1. IODP scientists hoped to characterize the subduction inputs on the Philippine Sea plate and prepare for later observatory installations for long-term monitoring of the seismogenic zone (Underwood et al. 2010). The expeditions which are the focus of this thesis are the eighth and ninth expeditions of the NanTroSEIZE program; IODP expedition 333 that occurred in 2010 and IODP expedition 338 in 2012. These two expeditions were part of Stages 2 and 3 of the NanTroSEIZE project and their primary goal was to collect core samples and logging while drilling (LWD) data on sites C0002, C0011, C0012, C0018, and C0021. The location of these drill sites in relation to drill sites from previous expeditions is shown in Figures 1 and 2.

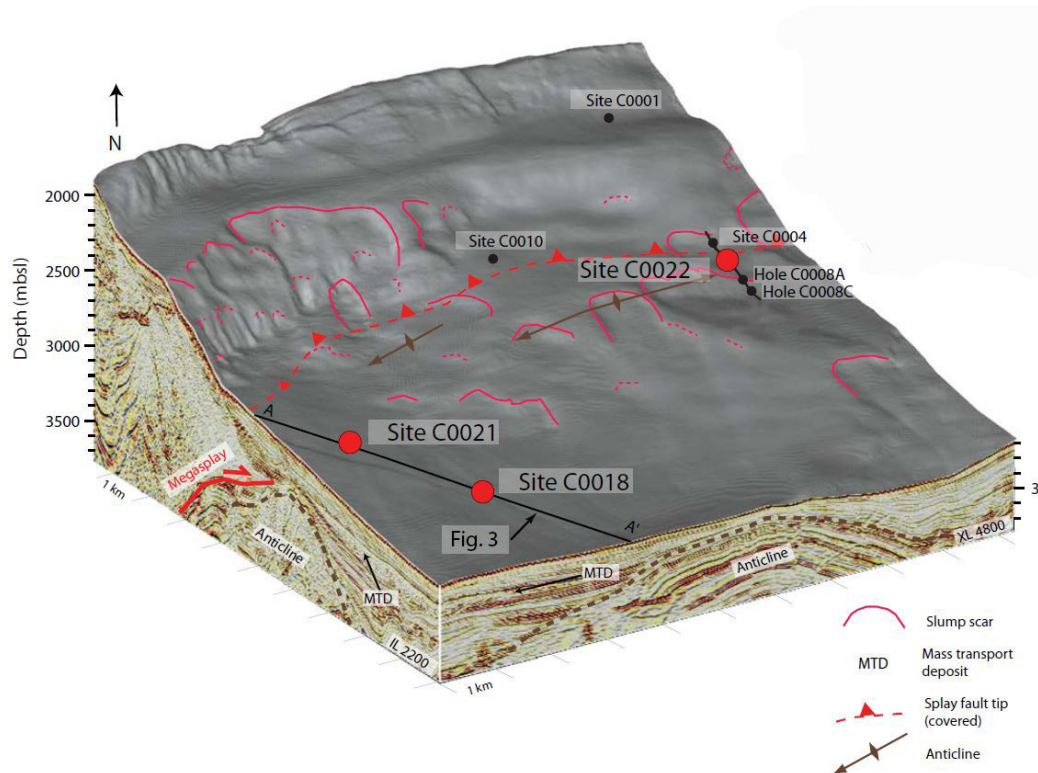


Figure 2: Detailed surface morphology and structure of the slope basin at the footwall of the splay fault. The sites in red shows IODP Expedition 338 sites in relation to the NanTroSEIZE Stage 1 and 2 sites which are shown in black. Solid black line through Site C0021 and C0018 is location of seismic line A-A' shown in Figure 3. IL: in-line, XL: cross-line. Modified from (Strasser et al. 2011).

A Slope Basin sequence seaward of the Megasplay Fault in the Nankai Trough, was drilled and sampled at Site C0018 to a depth of 314.2 mbsf during Expedition 333. Site C0018 was later logged during Expedition 338. Seismic correlation between C0021 and C0018 confirms that they are genetically related (Figure 3). A primary objective of Stage 2 was to define the Quaternary mass-movement event stratigraphy and to analyze physical properties in order to constrain sliding dynamics and tsunamigenic potential (McNeill et al. 2010). Expedition 338 also conducted LWD to 294 mbsf and coring to 194.5 mbsf at Site C0021 located 2 km northwest of site C0018 (Figure 1).

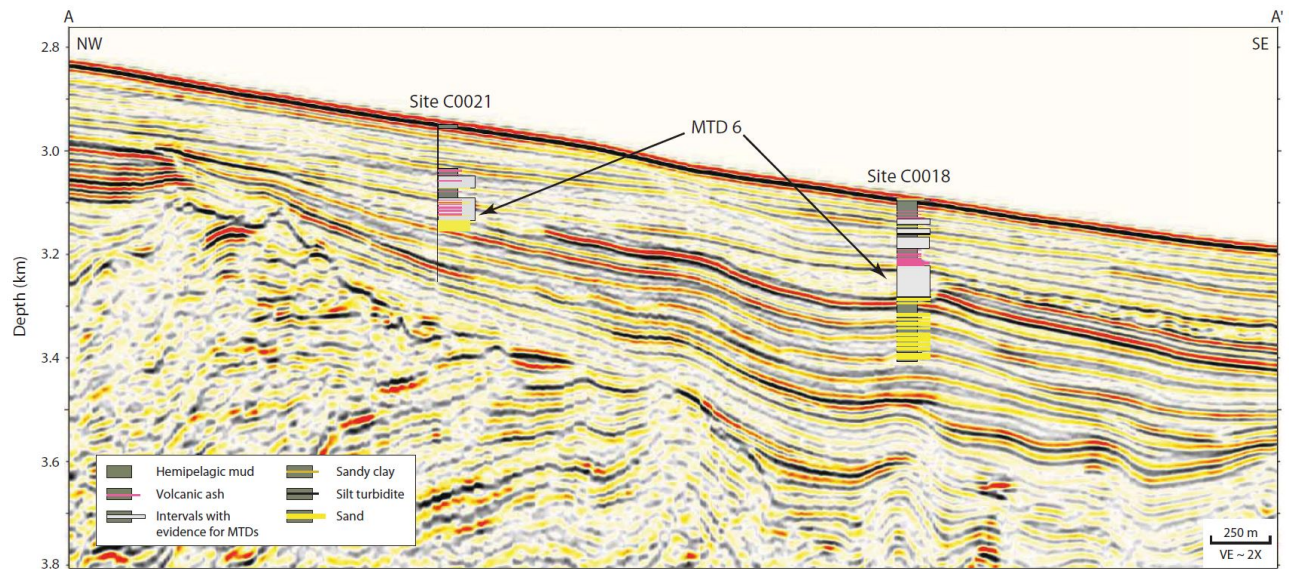


Figure 3: Seismic line A-A' through Sites C0021 and C0018 overlain with lithostratigraphic summary columns. Site C0018 indicated total logging depth (314.2 mbsf). VE: Vertical Exaggeration. Modified from (Strasser et al. 2014).

GEOLOGIC SETTING

The area of study for this thesis project focuses on the Nankai Trough region which is a submarine trough located off the southeast coast of Japan, which extends approximately 700-900 kilometers offshore (Figure 4). The trough was created by the subduction of the Philippine Sea Plate underneath the Eurasian Plate. Miyazaki and Heki (2001) estimated that the subduction rate of these two plates is occurring at a rate of 4.1 to 6.5 centimeters a year.

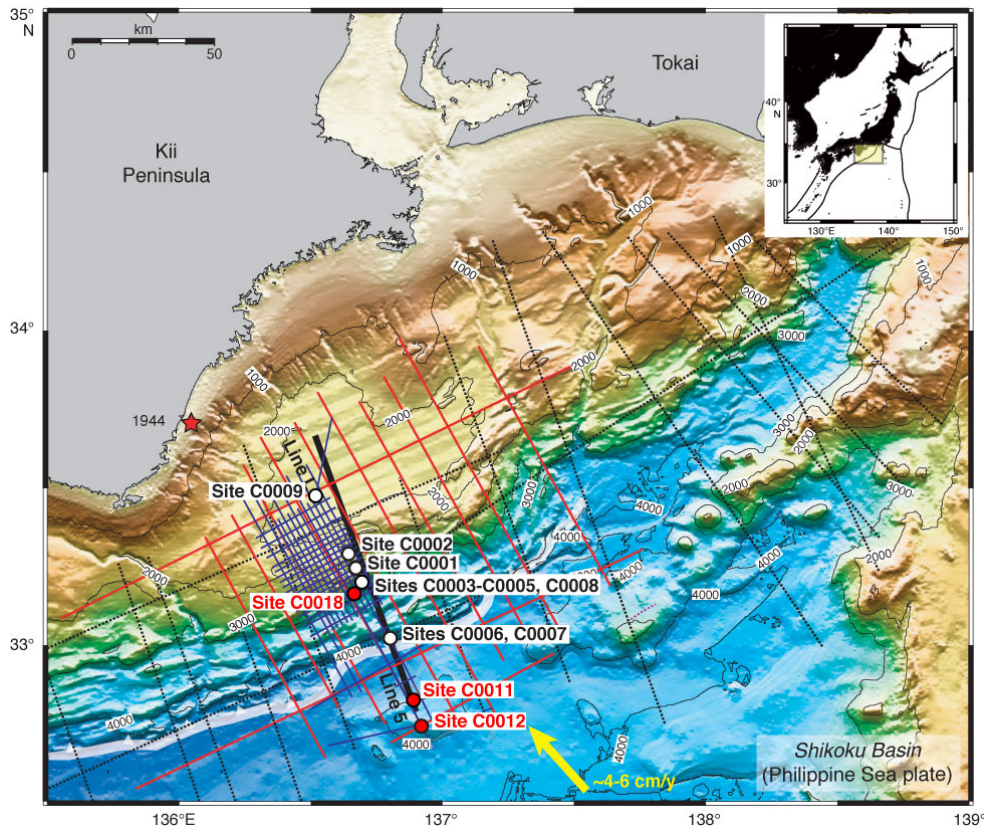


Figure 4: Map of the NanTroSEIZE region showing all IODP drill sites. Red Dots: Expedition 338 drill sites, Blue Dots: Expeditions 314-316 and 333 Stage 1 and 2 drill sites. Black Outline: regional 3-D seismic data coverage, Yellow Arrows: estimated far-field vectors between Philippine Sea plate and Japan (Seno et al.1993; Miyazaki and Heki. 2001).

Structural Evolution of the Nankai Trough

The subduction of the Philippine Sea Plate underneath the Eurasian Plate has created a wide accretionary prism (Figure 5). This large accretionary prism is broken up into two sections with a less active inner prism, and seaward of the Megasplay fault, an actively deforming outer prism (Moore et al. 2007). The inner

prism is capped by the Kumano Basin. The Kumano Basin is approximately 1.95 to 2 million years old and formed behind a ridge that was uplifted because of movement from the Megasplay fault (Moore et al. 2014). There is evidence for recent tectonic activity because both the basin strata and seafloor are cut by a series of normal faults (Moore et al. 2014).

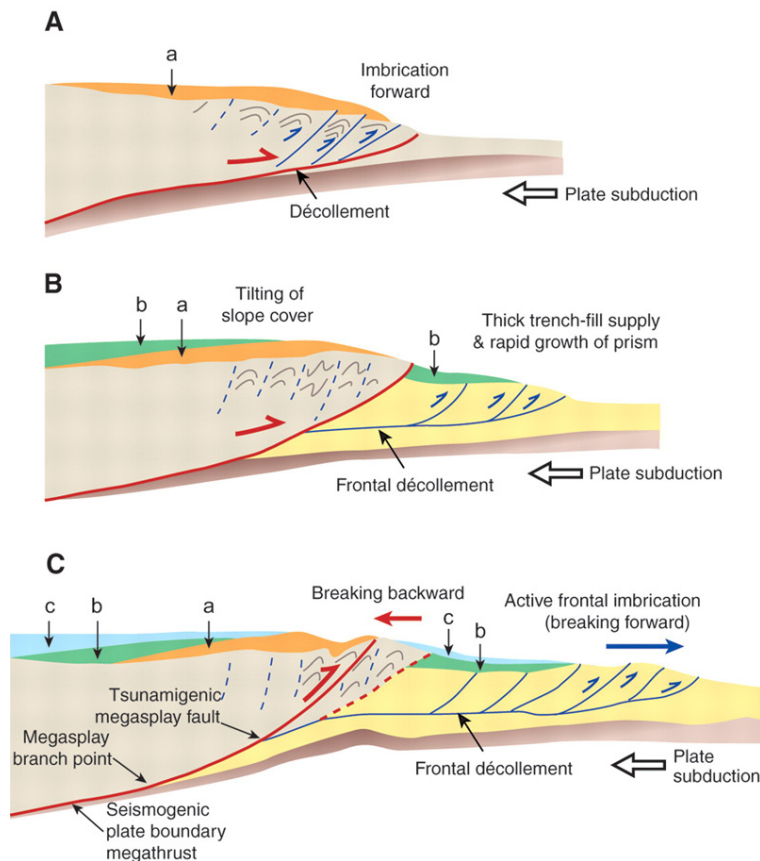


Figure 5: The images above show how the Nankai accretionary prism developed in the Kumano Basin area. After "normal" in-sequence thrusting and building of an accretionary prism, an out-of-sequence (splay) fault system broke through at the back of the prism. A, B, and C show the sequential sedimentary sequences. From Moore et al. 2007.

Past Tectonic Activity

The Nankai Trough is a seismically active zone with a high potential to produce large megathrust earthquakes. The large earthquakes this region has created in the past 1300 years have been well recorded. Historically, earthquakes in this region have had magnitudes as large as 9.0 on the Richter Scale with the oldest documented earthquakes being from 684 A.D. (Obana et al. 2003). Prior to 1361, these earthquakes had recurrence periods of approximately 200 years (Ando

1975). After 1361 the recurrence periods became even shorter with waves being about 100 years apart. These large earthquakes have been the cause of severe disasters in southwest Japan. The risk of future high intensity earthquakes (Figure 6) has caused the Nankai Trough to become one of the most studied seismic zones in the world.

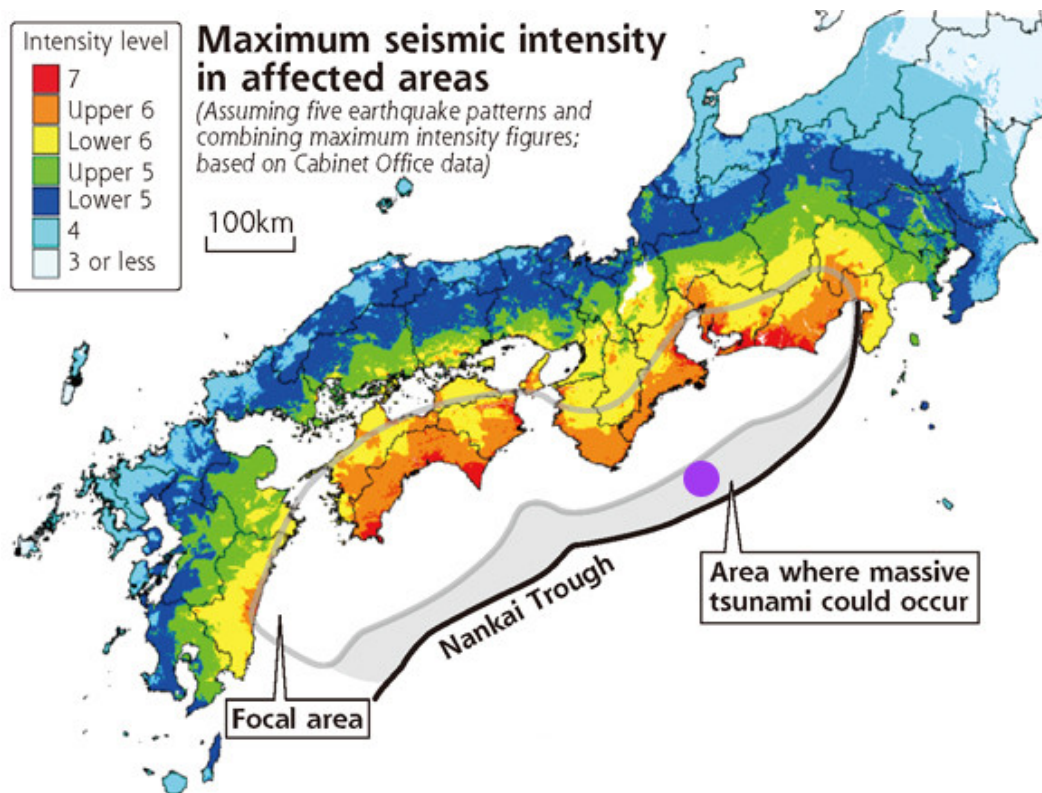


Figure 6: Map of Japan showing potential levels of seismic intensity from future tectonic activities related to the Nankai Trough. Purple Dot is the location of the study area. Edited from Cabinet Office, Government of Japan, (2006).

METHODS

Sampling methodology (Coring and Seismic Acquisition)

The cores used for grain size analysis were recovered by the riser-equipped *Chikyu* vessel during IODP Expedition 333. Coring was conducted during December 2010 and core recovery was excellent with very few operational problems. A hydraulic piston coring system was used to 153.85 meters below the seafloor. After the estimated MTD bottom was reached, the crew switched to an extended punch coring system which had variable recovery success that averaged 47.2% recovery. After the seventh core the crew switched to an extended shoe coring system which had a surprisingly good recovery average at 87.35%. Core quality assessment from X-ray computed tomography scans showed no major difference between the extended punch coring system and the extended shoe coring system (Expedition 333 Scientists, 2010).

The 3D seismic data were acquired by PGS Geophysical on the *M.V. Nordic Explorer*. The survey began in April 2006 and was completed in May 2006. The total area surveyed was 791 square kilometers in size. The survey utilized four 4500 meter streamers that were spaced 150 meters apart. The reported source type was a Soder G-gun and streamer type was a reduced diameter solid streamer. The seismic survey was sampled at a rate of 2 ms and had a 24 bit amplitude resolution.

Hydrometer Analysis

Particle size analysis was conducted at The Ohio State University using the standard hydrometer method for fine-grained samples (ASTM, 2007). Sawyer et al. (2008) and Moore et al. (2014) used similar hydrometer analyses on fine-grained sediments from within and without MTDs in the Ursa Basin and Nankai Trough, respectively.

Hydrometer analysis is based on Stokes' Law, which defines the terminal velocity of a spherical particle settling through a column of fluid. These particles settle at rates proportional to the size of the particle and to the difference in densities between the particle and the fluid through which it is settling. A

hydrometer measures the density of the mixture at a known depth below the surface. The density of the suspension is based on the specific gravity and amount of sediment. The density of the mixture decreases as the particles settle out of the suspension. Equation 1 provides the maximum particle diameter at the time of measurement (D in mm). Equation 2 provides the percentage of the original sample mass that is smaller than the particle diameter (mm) at the time of measurement, and thus, still in suspension (Germaine and Germaine, 2009). All variables are defined in Appendix 1.

$$(1) \quad D = \sqrt{\frac{18\mu}{\rho_w g (G_s - 1)}} * \sqrt{\frac{H}{t}}$$

Where:

H = distance particle falls (cm),

ρ_w = mass density of water (g/cm³),

G_s = specific gravity (dimensionless),

μ = viscosity of fluid (mPa · s),

g = acceleration due to gravity (cm/s²), and

D = Diameter of particle (mm).

$$(2) \quad N_m = [G_s / (G_s - 1)] \times (V / MD) \times \rho_c (r_m - r_{w,m}) \times 100$$

Where:

N_m = percent finer material at reading m (%),

V = volume of suspension (cm³),

MD = dry soil mass of hydrometer specimen (g),

ρ_c = mass density of water at the calibration temperature (g/cm³),

r_m = hydrometer reading in suspension at time t and temperature T (dimensionless)

$r_{w,m}$ = hydrometer reading in water with dispersant at the same temperature as for r_m (dimensionless), and

m = reading number.

Fifty (20-cm³ plug) samples were chosen from Site C0018 from 90.17 to 191.17 mbsf. Forty-one samples were collected from MTD-B. The remaining 9 samples were selected to provide some measure of the background non-MTD particle size distribution above and below the MTD. Moisture and density (MAD) data for Site C0018 revealed a range of grain densities between 2.55 g/cm³ and 2.77 g/cm³ and an average 2.73 g/cm³ for all 50 samples. Therefore a value of 2.7 was used in Eq. 1 and Eq. 2 and the error associated with using this value is < 5%. Sample preparation followed the ASTM hydrometer method (Germaine and Germaine, 2009). Each sample was removed from its sealed plastic shipping bag, weighed, and placed into a 250 mL beaker. The sample was then soaked for 12 hours in 125 mL of 5% solution of deflocculant [sodium hexametaphosphate (Na₆P₆·O₁₈)]. After each sample was disaggregated by a malt mixer for 2 minutes, and then was wet sieved through a 63 μ m screen to separate sand-size particles. The retained sand was dried and weighed for final percent sand calculations. The remaining <63 μ m slurry was transferred to a 1000 mL graduated cylinder and filled with deionized water to 1000 mL. One control cylinder was prepared using 5% aqueous solution of the dispersing agent and deionized water filled to 1000 mL. The hydrometer reading was measured and the temperature was monitored. The laboratory temperature control system maintained a stable temperature environment of 23.9°C and thus little variation in viscosity. However, if the temperature fluctuated by 1°C the resulting change in diameter is approximately 1%.

Before the start of each experiment, samples were mixed for one minute in the graduated cylinder using a plunger. The timer was started when the plunger was removed, and the hydrometer was inserted. Hydrometer readings were taken at 15, 30, and 60 seconds without the hydrometer being removed. After the 60

second reading, the hydrometer was removed and rinsed in deionized water. The sample was remixed and readings were again taken at 15, 30, and 60 seconds and averaged together. The hydrometer was again removed and rinsed.

[illegible]

Figure 7: Sample data sheet for hydrometer analysis. Hr = Hydrometer Reading, elapsed time = length of experiment before each recording, sample reading = recorded value from hydrometer, and effective depth = depth (L in Eq. 1) of hydrometer's center corrected for viscosity.

The hydrometer was then reinserted at 2, 4, 8, 16, and 32 minutes. Between measurements the hydrometer was removed. Each settling experiment continued until samples crossed the silt-clay boundary (2 μm), which typically occurred after a total settling time of 10 to 12 hours. The definition of the clay-silt boundary at 2 μm follows the standard used in many engineering studies. This is in contrast to the 4 μm boundary normally used in studies following the Shepard classification system. However, to be consistent with the data reported in Moore and Sawyer (2014) it was

thought best to stay with the 2 μm boundary. We recorded hydrometer readings to the nearest 0.1 g/L. An example hydrometer worksheet and graph are shown in Figures 7 and 8.

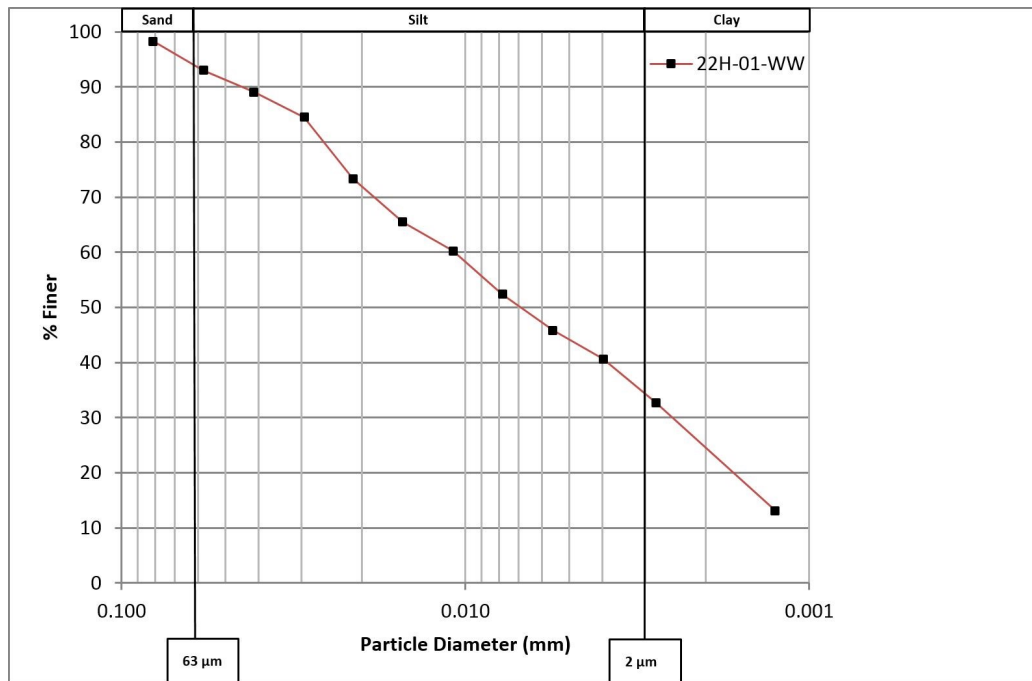


Figure 8: Sample Particle size distribution plot on a semilog scale (Sample 22H-01-WW: 176.54 mbsf).

After each sample crossed the silt-clay boundary, the sample dried in an oven and weighed for a final $<62.5 \mu\text{m}$ dry mass. The recorded final percentages were then plotted using a Shepard (1954) ternary diagram (Figure 9).

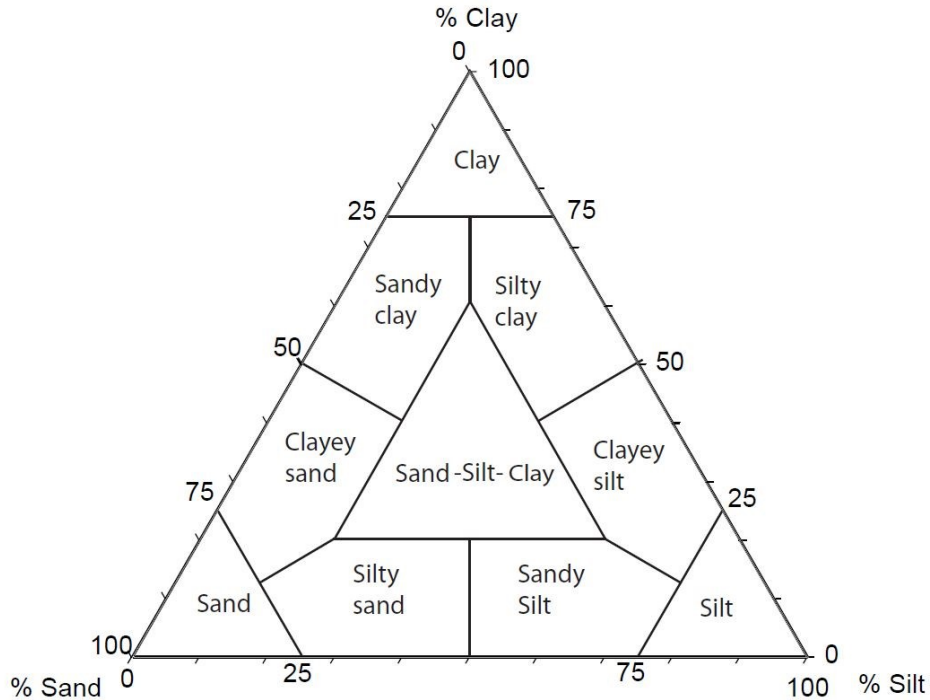


Figure 9: Shepard (1954) classification ternary diagram based on relative percentages of sand, silt, and clay.

Mapping in Kingdom

The 3D seismic mapping was done at The Ohio State University using the Kingdom Software®. The first goal was to map the top and base of MTD-B at Sites C0018 and C0021 (Figure 10) and throughout the entire Nankai Trough survey region. After MTD-B was mapped, it was necessary to determine the location of the pink volcanic ash horizon so it could be properly mapped. Based on grain size data and data from Expedition 333 Scientists (2010) it was determined that the pink ash layer was found to be located at approximately 188.45 to 190.65 mbsf within Site C0018. A strong reflection was also found directly below MTD-B which signals a significant change in acoustic impedance. The grain size analysis determined MTD-B is primarily clayey silt (Figure 12), which has a higher acoustic impedance than sandy volcanic ash. This indicates the presence of a negative reflector to match the pink volcanic ash horizon. With this information the pink volcanic ash layer was mapped away from the control site. In addition, I mapped another MTD found in the survey area that was located directly above the pink volcanic ash.

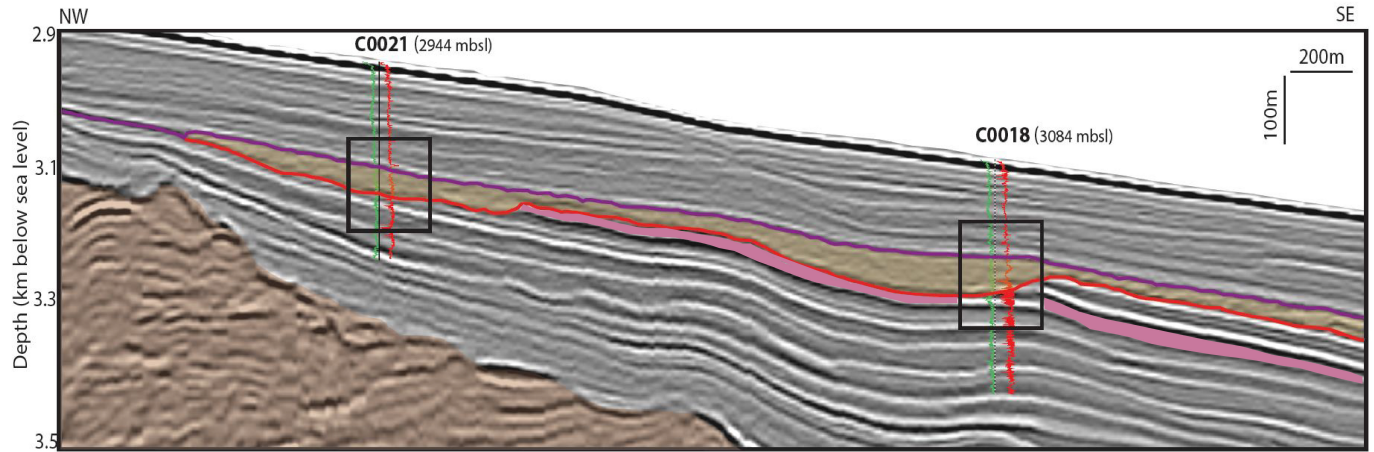


Figure 10: Seismic Data from Nankai Trough survey. Figure shows wells C0021 and C0018 both drilled through MTD-B (brown). Mapped pink horizon under Site C0018 contains Pink Volcanic Ash layer.

Data interpretation

Even though the hydrometer experiments conducted on Sites C0018 and C0021 followed the same ASTM (2007) method a reproducibility test was conducted to affirm results would have no significant error. Site C0021 hydrometer testing was previously conducted at the University of Kentucky (Moore and Sawyer, 2014) prior to hydrometer testing on Site C0018 at the Ohio State University (this study). For the reproducibility test sample 9H-1-WW (147.mbsf) from Site C0021 was selected and a second hydrometer test was run on the core material. The results were graphically compared (Figure 11) and found to be statistically similar with only 3.9% error between the two measurements calculated. The low error means that the location of the hydrometer experiments in no way significantly altered the grain size data obtained.

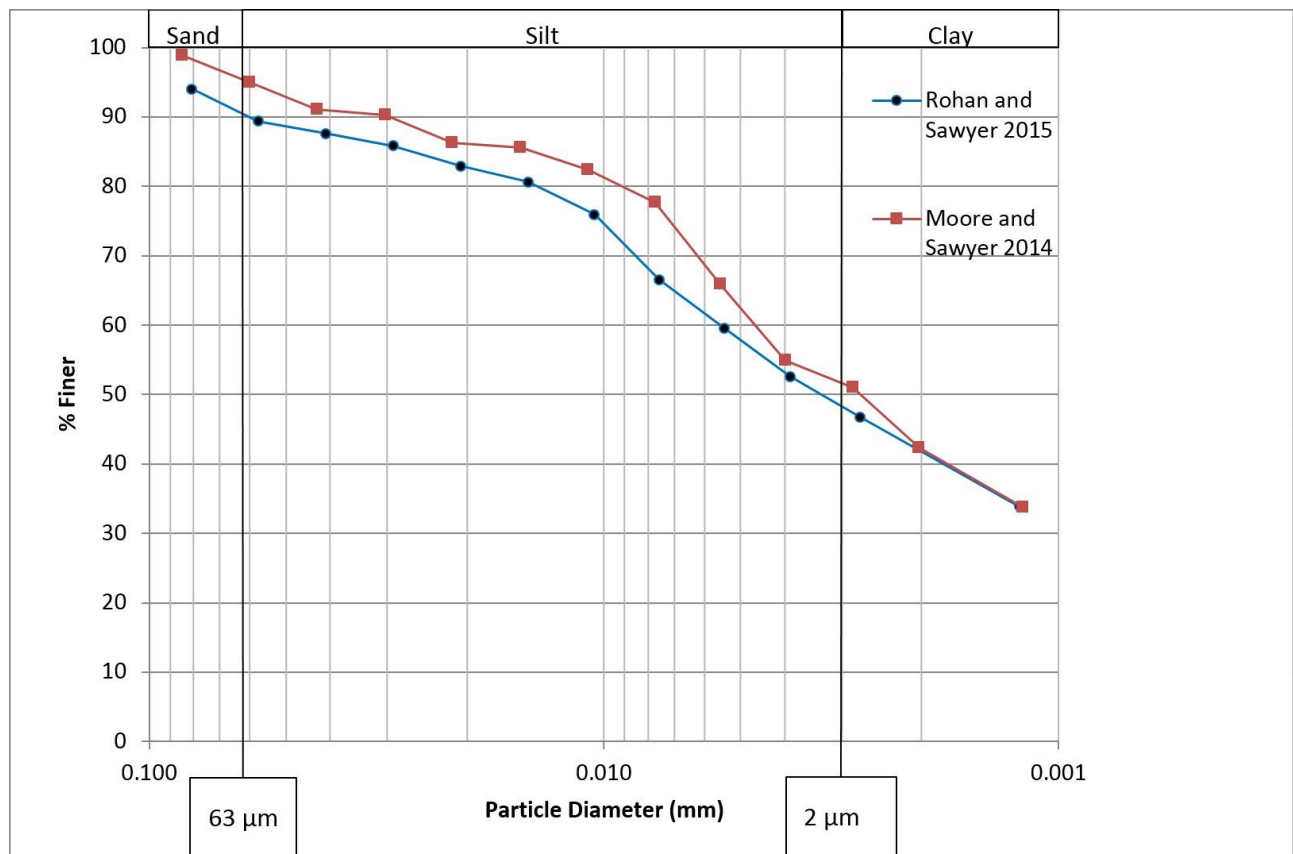


Figure 11: Reproducibility test (Sample 9H-1-WW: 147.18 mbsf) measured at the Ohio State University (this study) and University of Kentucky (Moore and Sawyer, 2014). 3.9% Error Calculated.

RESULTS

Grain Size Distribution across the Mass Transport Deposit

In Appendix 2 weight percent sand, silt, and clay for all samples from well site C0018. The particle size distributions are plotted on a ternary diagram according to the classification of Shepard (1954) (Figure 12), and as a down-core profile of weight percent sand, silt, and clay against LWD gamma ray and resistivity (Figure 13).

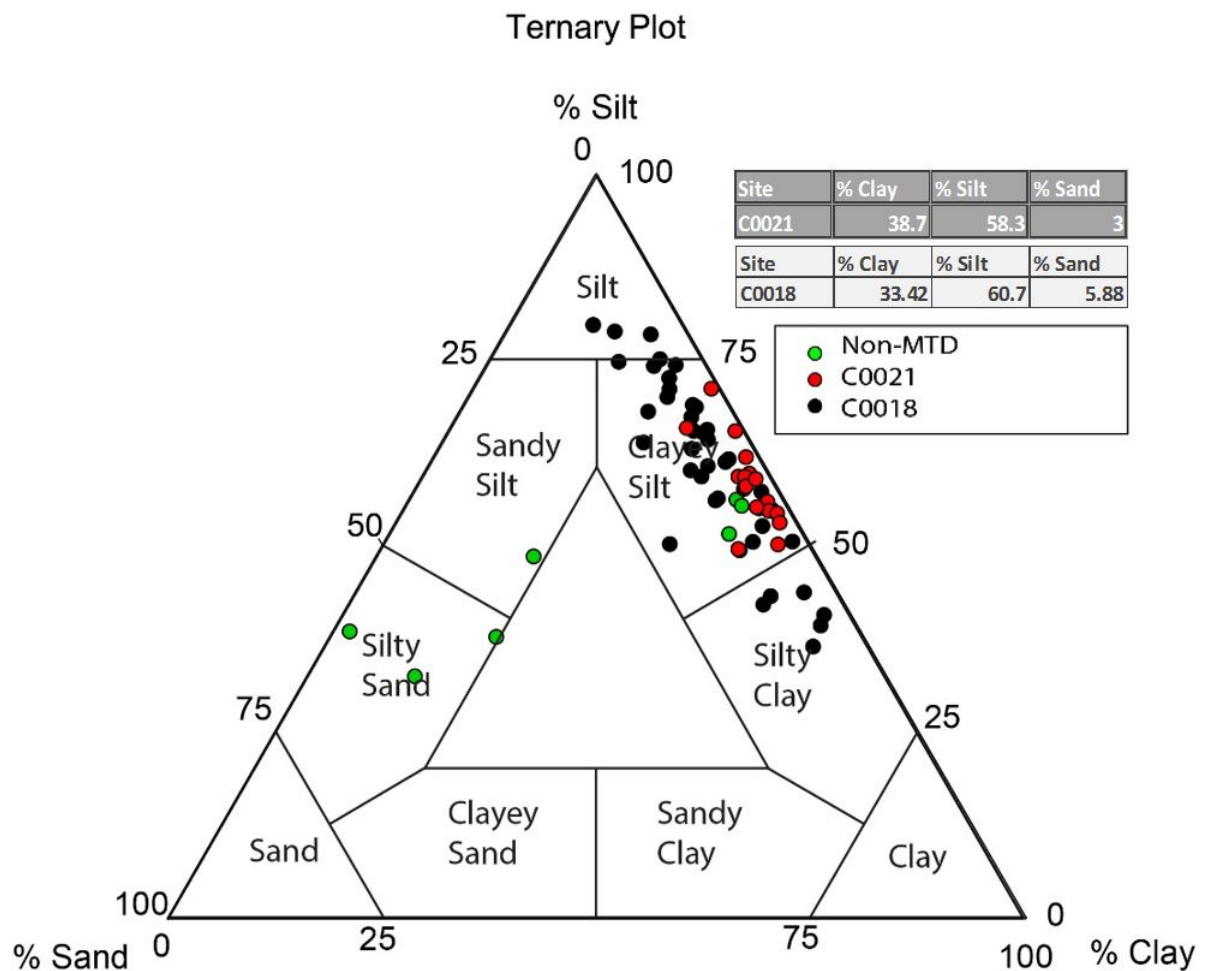


Figure 12: Combined hydrometer results for 31 samples, Site C0021 (Moore and Sawyer, 2014) in red and 50 samples, Site C0018 in black. Plotted on a Shepard (1954) ternary diagram.

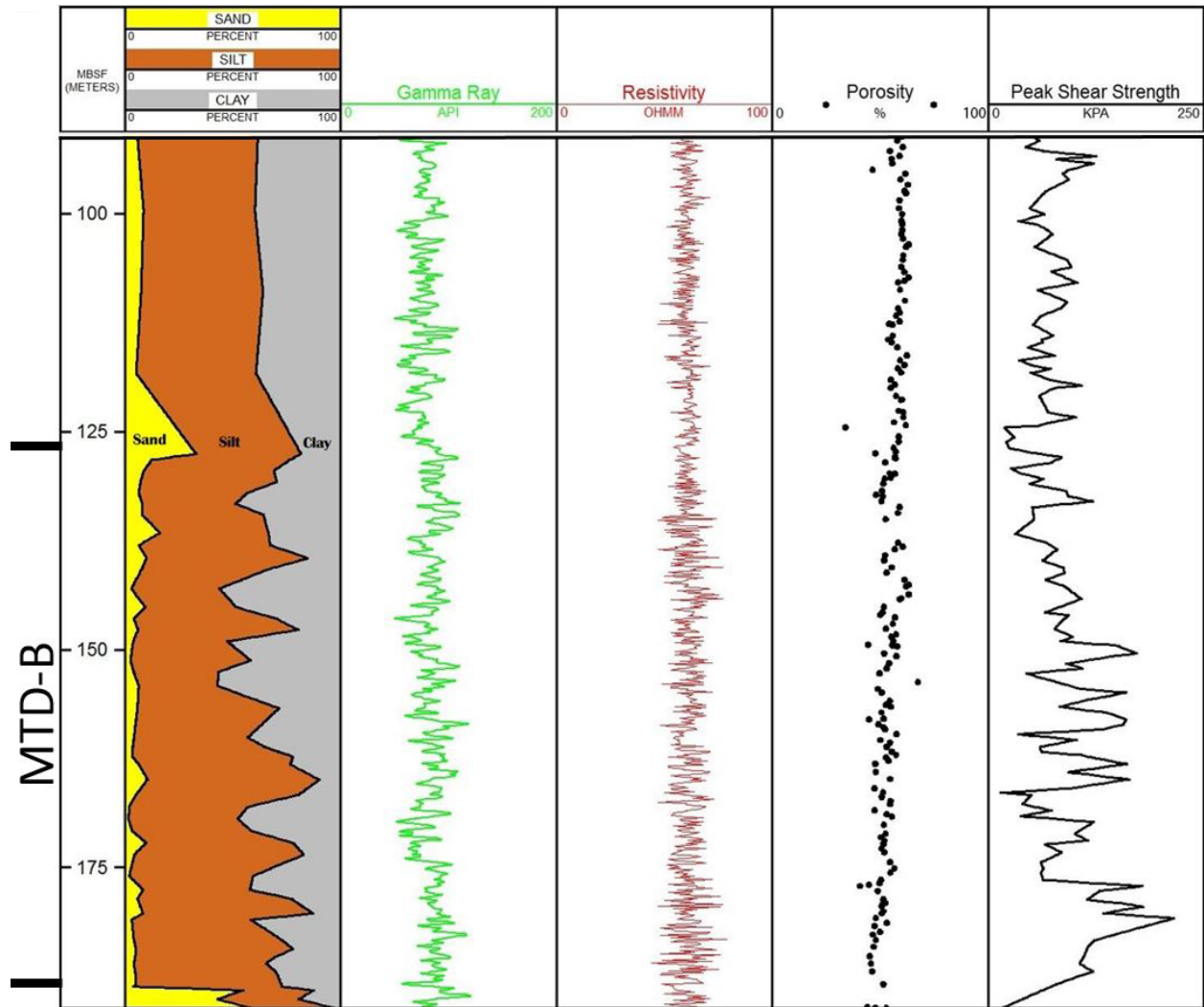


Figure 13: Plot of particle size distribution with LWD gamma ray, resistivity, porosity, and peak shear strength, Hole C0018. LWD log data from (IODP Expedition 333 Scientists, 2010).

The ternary classification defines two major lithologies (silty clay and clayey silt) and four minor (silt, sandy silt, silty clay and silty sand) (Figure 12). Seventy-eight percent (39 of 50) of the samples are clayey silt; 15% are silty clay, and 7% are minor lithologies. Overall, clay content decreases down-core, and there was a significant increase of sand at the detachment surface of the landslide. No obvious particle size differences occur between Site C0018 and C0021 samples (Figure 12). However, samples from Site C0018 have more noticeable down core variations (Figure 13). Another noticeable feature is the large spike in sand grains at the bottom of the MTD in well C0018. This correlates with a large volcanic deposit

called the pink volcanic ash horizon, which cannot be seen at Site C0021 (Figure 14). This volcanic ash layer was identified during shipboard description of the core samples and has been measured to be 1-1.5 m thick by IODP 333 scientists.

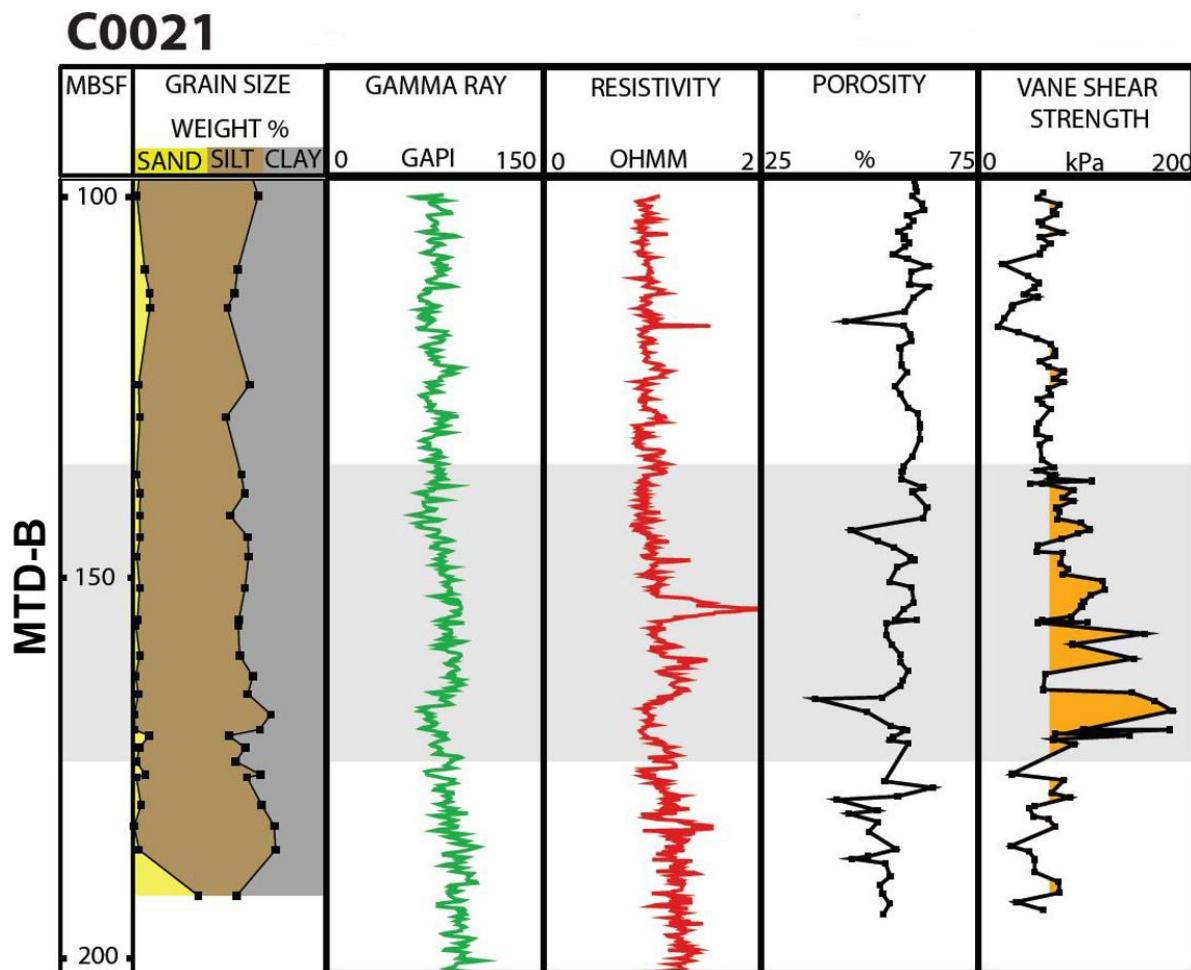


Figure 14: Particle Size data and LWD gamma ray, resistivity, porosity, and Shear Strength logs from Site C0021 (Moore and Sawyer, 2014). Section containing MTD-B is shaded in gray.

The Pink Volcanic Ash Horizon

The large volcanic ash layer that sits just below MTD-B corresponds with the Pink Volcanic event that is dated to be 0.99-1.05 million years old and from Kyushu Island, Japan (Hayashida et al. 1996). Figure 15 provides insight into why the volcanic ash was not found when conducting a grain size analysis on site C0021. As the seismic data shows in Figure 15 the volcanic ash horizon in pink has been cut out by the base of MTD-B just before Site C0021.

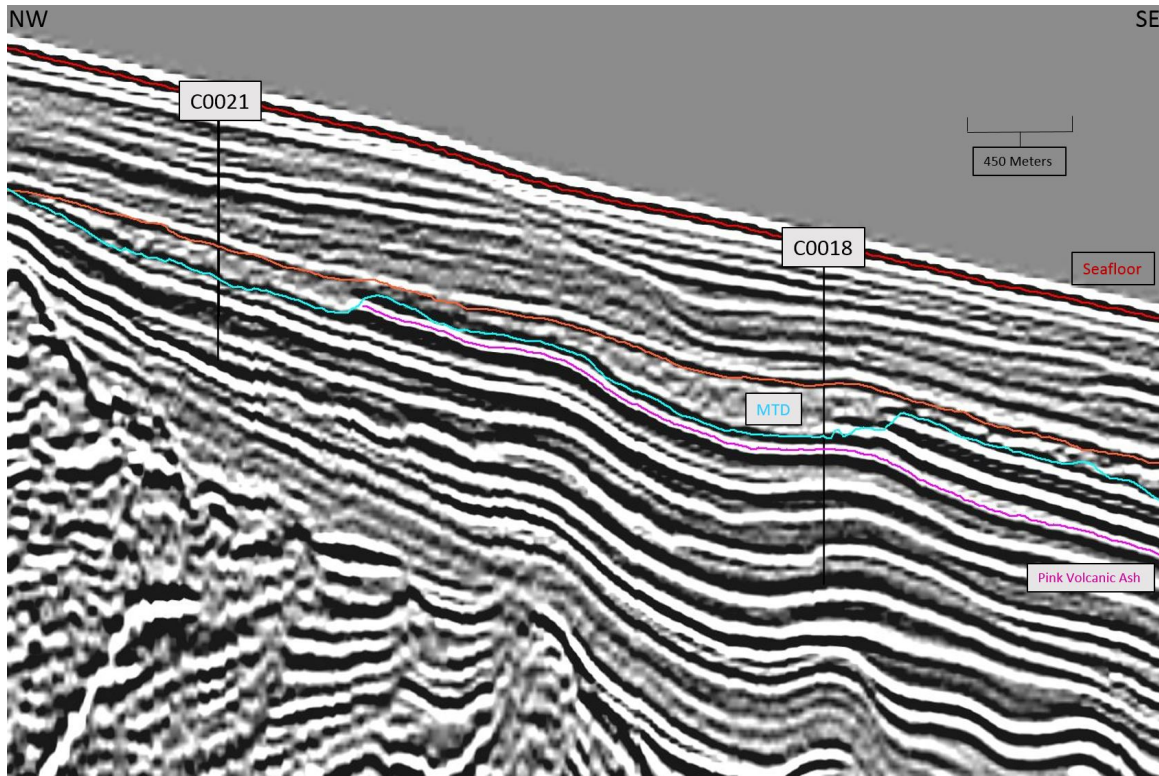


Figure 15: The seismic data shown above shows the Pink volcanic ash layer (pink line) being cut out by the sediments of the MTD (blue line) before reaching well site C0021.

The pink ash may have had a role in mobilizing the submarine landslide event that created this MTD. The seismic data shows us widespread extent of the volcanic ash suggesting that the pink ash can expected to be found throughout the surveyed region of Nankai Trough. While there were smaller landslides in the proximity of the pink volcanic ash layer one larger MTD also cuts out the pink volcanic ash layer in the seismic survey. This MTD was also mapped in the seismic survey. Seismic data through sites C0018 and C0021 show that the landslide has displaced fragments of the pink volcanic ash layer that it may have slide on. With both MTD-B and the surficial landslide mapped, a 3D model was created with the Kingdom Software ® (Figure 16).

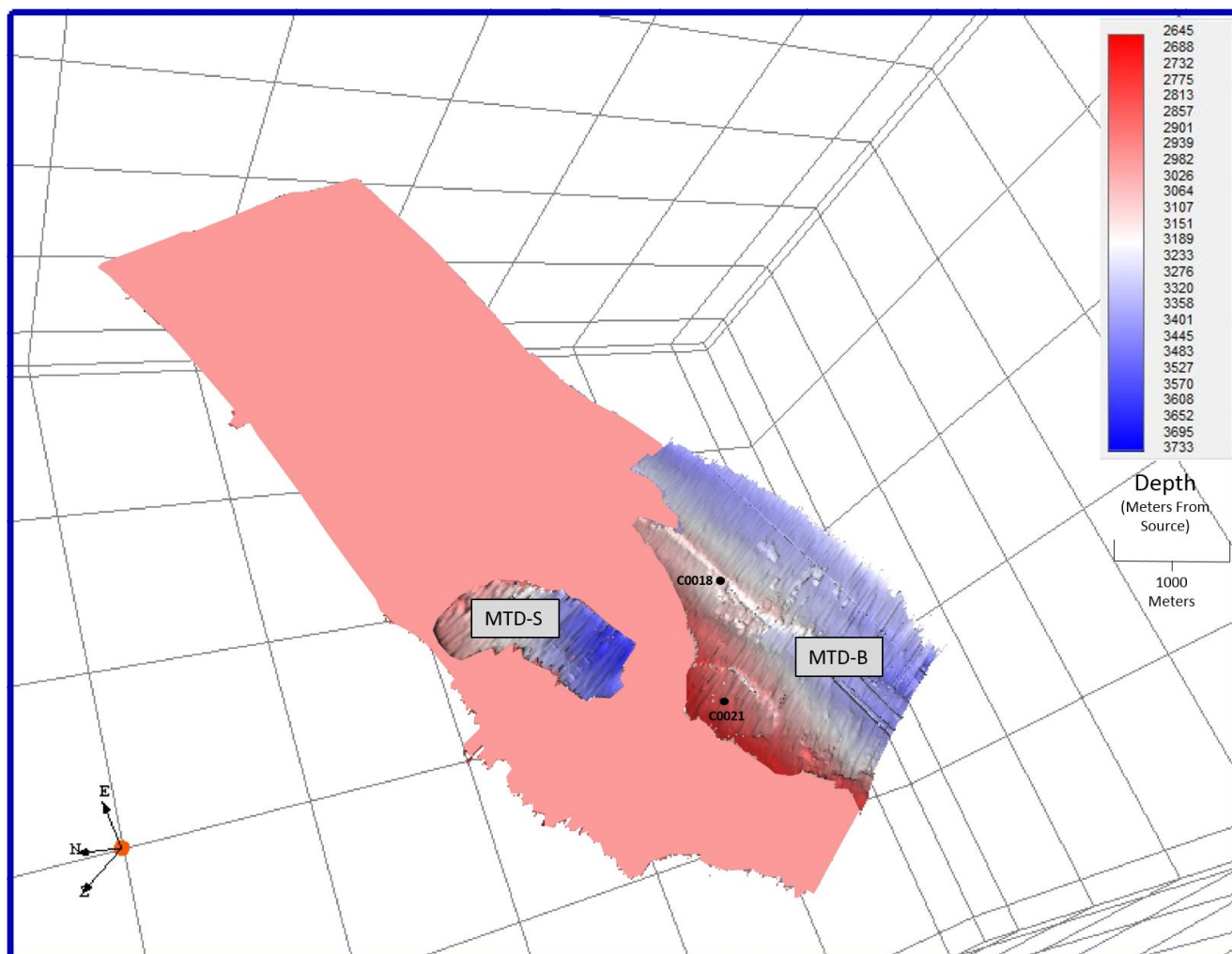


Figure 16: 3D Model showing the pink volcanic ash layer (pink) overlain by MTD-B, containing Sites C0018 and C0021 (black dots), and another large surficial MTD (MTD-S) shown to the left.

DISCUSSION

Variation of Grain Size in Grain Size Analyses

One of the goals of this study was to examine a single submarine landslide deposit (MTD-B) from two coring sites (C0018 and C0021). With both particle size analysis experiments completed we now have the rare opportunity study a landslide from two well sites that are roughly 2 kilometers apart. The core analyzed from Site C0018 had 41 core samples from within MTD-B. The average grain sizes from those samples were 61% silt, 33% clay, and 6% sand. This was similar to the grain size data obtained from the 18 core samples analyzed in MTD-B from site C0021. Similarly, the grain sizes from MTD-B at site C0021 averaged to 59% silt, 38% clay, and 3% sand. The average grain size data from both sites C0021 and C0018 look very similar. However, when the grain size data are plotted a clear variation in grain size data occurs at site C0018 while site C0021 represents more limited variability in grain size (Figure 14) with increasing depth through MTD-B.

There are multiple possibilities for what could have caused this difference in the grain size data sets. One possible explanation is the landslide evolved from a slide to a debris flow and then to a turbidity current. This evolution takes place with increasing fining of grains and entrainment of water (Masson et al. 2006). During this process the sediment is rapidly mixed with seawater as it moves downslope. This could suggest that the details of this mass flow that were deposited at Site C0018 may have been slightly different than what was deposited at Site C0021. However, this process of large turbidity currents mixing with seawater is a poorly understood process (Talling et al. 2002). Without complete understanding of the process it is difficult to accurately determine that this was a definite cause for the different data patterns between the two sites.

The grain size experiments for this study at Site C0018 had the 42 samples from within MTD-B and only 8 core samples located above and below (pink volcanic ash) the MTD. This differs from the grain size analysis performs on samples from Site C0021, that only had 18 samples within MTD-B. This raises the question of

whether a similar pattern would have been seen if the same number of grain size experiments were conducted for Site C0021 within MTD-B.

Potential Causes for Destabilizing the Sea Floor

In this study we hoped to gain more information about both the depositional history and morphology of MTD-B. The grain size analysis at Site C0018 provided insight into a likely detachment surface for the submarine landslide (Pink Volcanic Ash). Figure 17 models how the submarine landslide might have progressed after a trigger event (earthquake/overpressure).

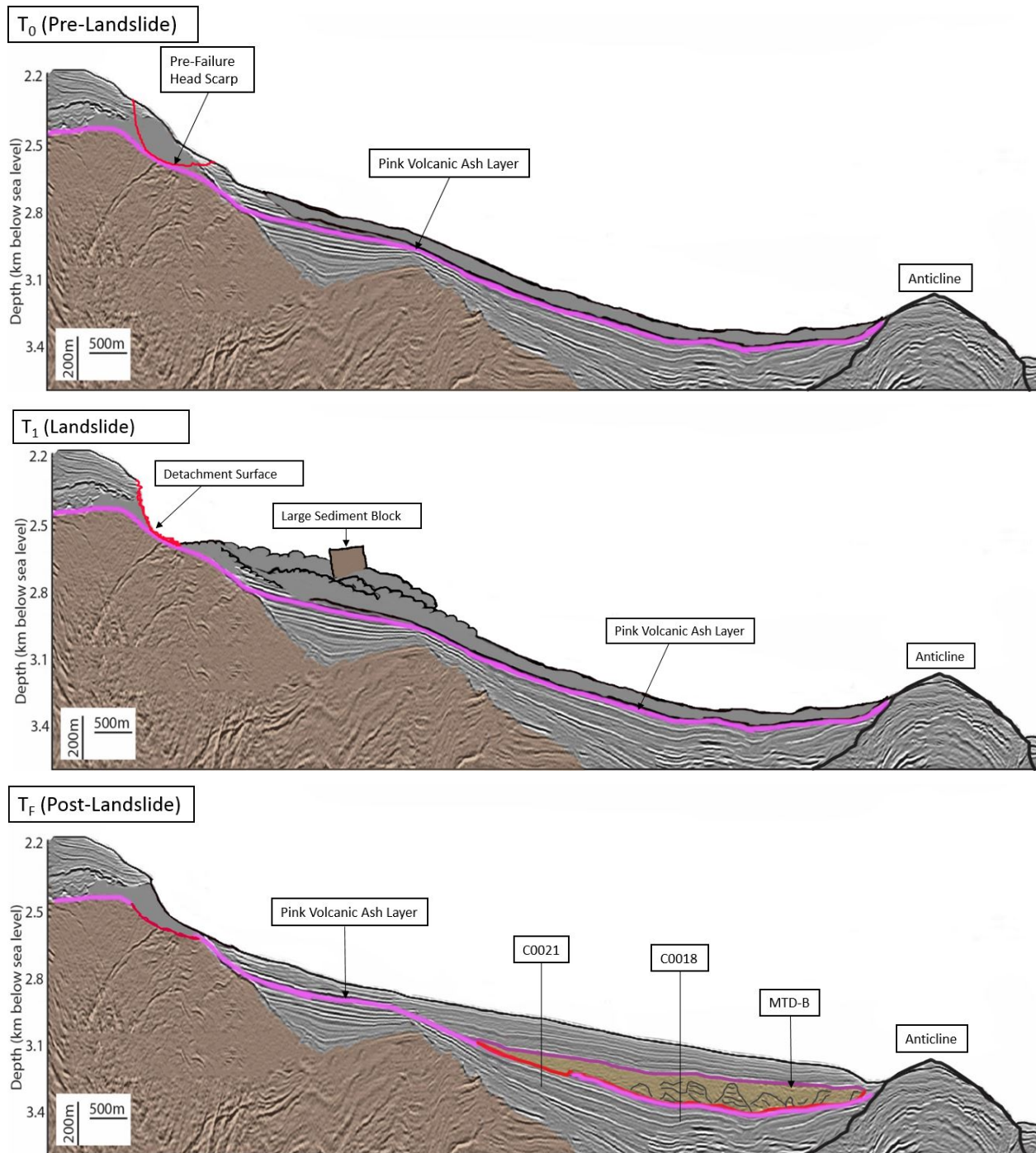


Figure 17: Model of Depositional History of MTD-B with the pink volcanic ash horizon being the primary detach surface.

Role of the Volcanic Ash in Mobilizing Landslides

The pink volcanic ash is dated to be 1.05 Ma on land and lies at approximately 183.8-190.65 mbsf at Site C0018 (IODP Expedition 333 Scientists,

2010). Figure 18 shows a smear slide photo of the volcanic ash which was microscopically characterized by Expedition 333 scientists.

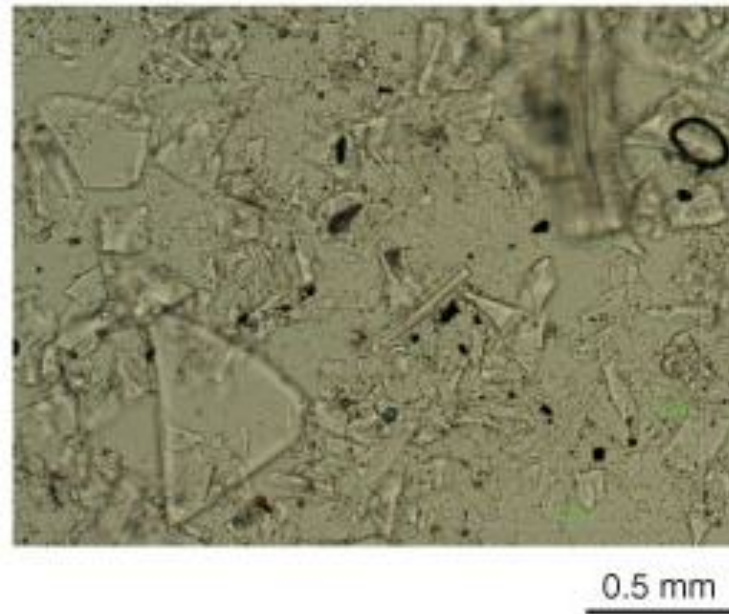


Figure 18: Smear slide photo (Sample C0018-23H-3) that shows microscopic features such as bubble wall volcanic glass shards and minor amount of hornblende (IODP Expedition 333 Scientists, 2010).

This volcanic ash layer is regionally widespread and mapped using 3D seismic analysis allowing us to learn more about the horizon. The ash layer is a distinctive thick, sand-sized volcanic ash. The map of the horizon showed that this horizon was not only at the base of MTD-B, but also at the base of another landslide in the study area. Figure 19 shows this MTD that also is deposited on top of the pink volcanic ash horizon.

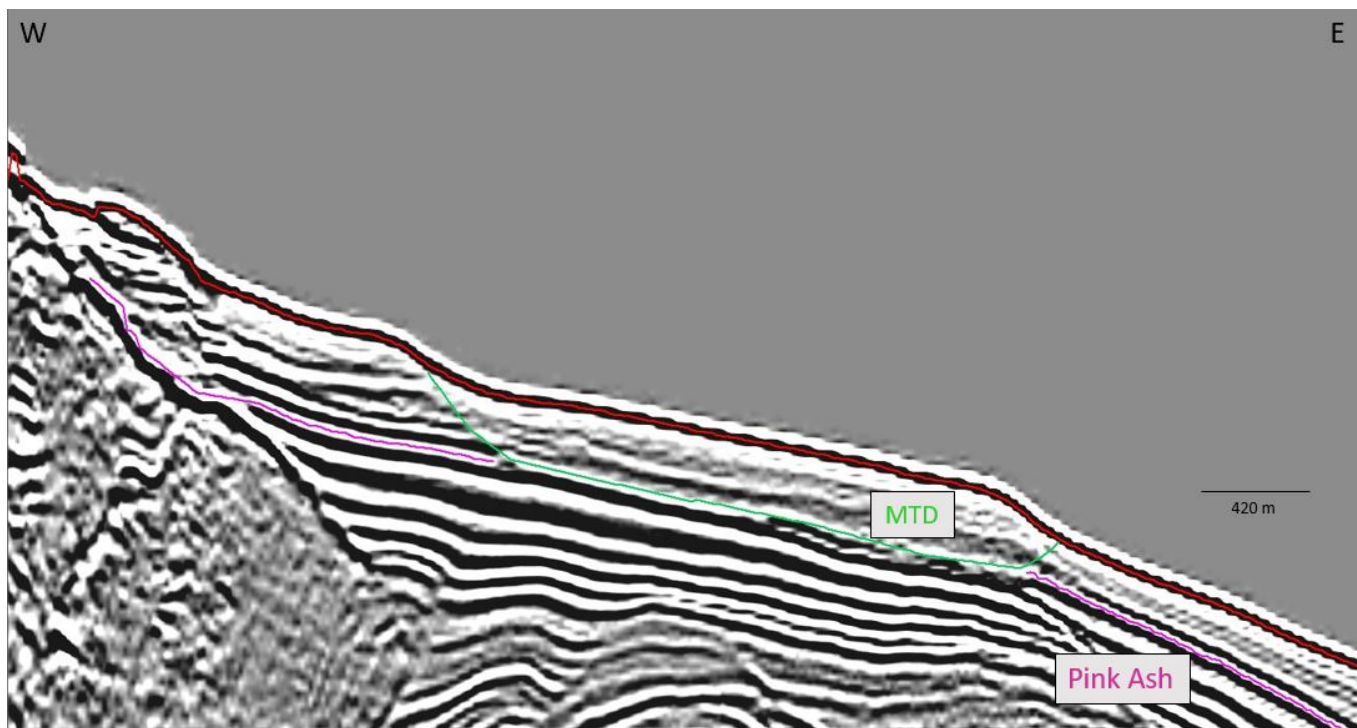


Figure 19: Seismic data showing surficial landslide deposit cutting out the pink volcanic ash layer.

CONCLUSIONS

My main conclusions are:

- Hydrometer analysis determines that at Site C0018, MTD-B is 78% clayey silt material.
- Averages for grain size data from Site C0018 and Site C0021 are similar within MTD-B.
- A thick, Pink volcanic ash horizon underlies MTD-B at site C0018 that can be mapped in seismic data has the potential to have been the primary detachment surface for MTD-B.
- Seismic data shows that this volcanic ash layer is regionally widespread inside of the seismic survey.
- The Pink ash underlies another MTD that can be mapped in seismic data throughout the study area.
- The Pink Volcanic Ash horizon may have been a weak layer that allowed several landslides to mobilize.
- On a broader scale, ash beds may be responsible for creating weak layers along which landslides can fail in other volcanic regions.

RECOMMENDATIONS FOR FUTURE WORK

Possible future research could include an expansion of the seismic survey in the Nankai Trough to find other MTDs that could be underlain by the pink volcanic ash horizon. Moore et al. (2016) have further examined MTDs in the Nankai region through the use of seismic data and discovered MTDs there may be in proximity to the Pink Volcanic Ash layer. This research could be expanded to look at other volcanic horizons in the area and if many were found underlying MTDs there could be a potential mechanistic relationship between submarine landslides mobilization in the region and deposition on volcanic ash. Additional well sites in the Nankai Trough could provide core samples to confirm seismic mapping of the pink volcanic ash outside of the well sites in the seismic survey.

REFERENCES CITED

- Ando, M. (1975) Source Mechanisms and Tectonic Significance of Historical Earthquakes along the Nankai Trough, Japan. *Tectonophysics* 27.2 (1975): 119–140.
- Alves, T. M., Kurtev K., Moore G., and Strasser M. (2014) Assessing the Internal Character, Reservoir Potential, and Seal Competence of Mass-transport Deposits Using Seismic Texture: A Geophysical and Petrophysical Approach. *Bulletin AAPG Bulletin* 98.4: 793–824.
- ASTM International, (2007) Standard test method for particle-size analysis of soils (Standard D422-63[2002]). In *Annual Book of ASTM Standards* (Vol. 04.08): Soil and Rock (I): West Conshohocken, PA (Am. Soc. Testing and Mater.), 10–17
- Cabinet Office, Government of Japan. (2006) Maximum Seismic Intensity in Affected Areas. Cabinet Office Documents.
- Expedition 333 Scientists. (2010) NanTroSEIZE Stage 2: Subduction Inputs 2 and Heat Flow. Integrated Ocean Drilling Program Management International, Inc.
- Germaine, J. T. and A. V. Germaine (2009) *Geotechnical Laboratory Measurements for Engineers*. Hoboken, NJ, John Wiley & Sons, Inc.
- Haflidason, H., Sejrup, H. P., Nygard, A., Meinert, J., Bryn, P., Lien, R., Forsberg, C. F., Berg, K. & Masson, D. G. (2004) The Storegga slide: architecture, geometry and slide development. *Mar. Geol.* 213, 201–234.
- Hampton, M. A., Lee, H. J. & Locat, J. (1996) Submarine landslides. *Rev. Geophys.* 34, 33–59.
- Hayashida, A., H. Kamata, and T. Danhara. (1996) Correlation of Widespread Tephra Deposits Based on Paleomagnetic Directions: Link between a Volcanic Field and Sedimentary Sequences in Japan. *Quaternary International* 34–36: 89–98.
- Henry, P., T. Kanamatsu, K. T. Moe, and M. Strasser. (2012) IODP Expedition 333: Return to Nankai Trough Subduction Inputs Sites and Coring of Mass Transport Deposits. *Scientific Drilling Sci. Dril.* 14: 4–17.
- Masson, D. G., C. B. Harbitz, R. B. Wynn, G. Pedersen, and F. Lovholt. (2006) Submarine Landslides: Processes, Triggers and Hazard Prediction. *Philosophical Transactions of the Royal Society A: Mathematical, Physical and Engineering Sciences* 364.1845: 2009–2039.
- McNeill, L., Saffer D., Byrne T., Araki E., Toczko S., Eguchi N., and Takahashi K. (2010) IODP Expedition 319, NanTroSEIZE Stage 2: First IODP Riser Drilling Operations and Observatory Installation Towards Understanding Subduction Zone Seismogenesis. *Scientific Drilling* 10, September 2010.

- Miyazaki, S. and Heki, K. (2001) Crustal velocity field of southwest Japan: Subduction and arc-arc collision. *Journal of Geophysical Research* 106: 0148–0227.
- Moore, G. F., N. L. Bangs, A. Taira, S. Kuramoto, E. Pangborn, and H. J. Tobin. (2007) Three-Dimensional Splay Fault Geometry and Implications for Tsunami Generation. *Science* 318.5853: 1128–131.
- Moore, G. F., and Strasser M. (2016) Large Mass Transport Deposits in Kumano Basin, Nankai Trough, Japan. *Submarine Mass Movements and Their Consequences Advances in Natural and Technological Hazards Research*: 371–79.
- Moore, G. F., K. Kanagawa, M. Strasser, B. Dugan, L. Maeda, and S. Toczko. (2014) IODP Expedition 338: NanTroSEIZE Stage 3: NanTroSEIZE Plate Boundary Deep Riser 2. *Scientific Drilling Sci. Dril.* 17: 1–12.
- Moore, Z., and Sawyer D. (2014) Data Report: Particle Size Analysis of Nankai Trough Sediments, IODP Expedition 338 Site C0021. *Proceedings of the IODP*
- Obana, K., S. Kodaira, Y. Kaneda, K. Mochizuki, M. Shinohara, and K. Suyehiro. (2003) Microseismicity at the Seaward Updip Limit of the Western Nankai Trough Seismogenic Zone. *J. Geophys. Res. Journal of Geophysical Research: Solid Earth* 108.B10
- Sawyer, D. E., Flemings P., Buttles J., and Mohrig D. (2012) Mudflow transport behavior and deposit morphology: Role of shear stress to yield strength ratio in subaqueous experiments. *Marine Geology* 307–310: 28–39.
- Sawyer, D. E., R. Jacoby, P. B. Flemings, and J. T. Germaine (2008) Data Report: Particle Size Analysis of Sediments in the Ursa Basin, IODP Expedition 308 Sites U1324 and U1322, Northern Gulf of Mexico, in *Proc. IODP*, 308 doi: 10.2204/iodp.proc.308.205.2008
- Seno, T., Stein, S. and Gripp, A.E. (1993) A model for the motion of the Philippine Sea plate consistent with NUVEL-1 and geological data. *Journal of Geophysical Research*, 98: 0148–0227.
- Shepard, F. P. (1954) Nomenclature based on sand-silt-clay ratios, *Journal of Sedimentary Petrology*, 24, 151–158.
- Strasser, M., B. Dugan, K. Kanagawa, G.F Moore, S. Toczko, L. Maeda, and the Expedition 338 Scientists, (2014) *Proceedings IODP, 338: (Integrated Ocean Drilling Program)*.
- Strasser, M., G. F. Moore, G. Kimura, A. J. Kopf, M. B. Underwood, J. Guo, and E. J. Screaton (2011) Slumping and mass transport deposition in the Nankai fore arc: Evidence from IODP drilling and 3-D reflection seismic data, *Geochemistry, Geophysics, Geosystems*, 12(5)

- Talling, P. J., J. Peakall, R. S. J. Sparks, C. O. Cofaigh, J. A. Dowdeswell, M. Felix, R. B. Wynn, J. H. Baas, A. J. Hogg, D. G. Masson, J. Taylor, and P. P. E. Weaver. (2002) Experimental Constraints on Shear Mixing Rates and Processes: Implications for the Dilution of Submarine Debris Flows. Geological Society, London, Special Publications 203.1:89–103.
- Underwood, M.B., Saito, S., Kubo, Y., and the Expedition 322 Scientists. (2010) Expedition 322 summary. In Saito, S., Underwood, M.B., Kubo, Y., and the Expedition 322 Scientists, Proc. IODP, 322: Tokyo (Integrated Ocean Drilling Program Management International, Inc.).
- Yamada, Y., K. Kawamura, K. Ikehara, Y. Ogawa, R. Urgeles, D. Mosher, J. Chaytor, and M. Strasser. (2012) Submarine Mass Movements and Their Consequences, in *Submarine Mass Movements and Their Consequences: 5th International Symposium*, pp. 1–12.

APPENDIX

Table 1: List of Variables

Variable	Meaning	Dimensions	Value
H	Distance particle falls	cm	Variable
ρ_w	Mass density of water	g/cm^3	0.9975412
G_s	Specific gravity	Dimensionless	2.70
μ	Viscosity of fluid	$\text{mPa}\cdot\text{s}$	9.53×10^{-6}
t	Time for fall	Minutes	Variable
g	Acceleration due to gravity	cm/s^2	980
D	Diameter of particle	mm	Variable
N_m	Percent finer material at reading m	Percent	Variable
V	Volume of suspension	cm^3	1000
M_D	Dry soil mass of hydrometer specimen	g	Variable
ρ_c	Mass density of water at the calibration temperature	g/cm^3	0.9975412
r_m	Hydrometer reading in suspension at time, t , and temperature, T	Dimensionless	Variable
$r_{w,m}$	Hydrometer reading in water with dispersant at the same temperature as for r_m	Dimensionless	1004.0
m	Reading number		

Table 2: Data from Particle size analysis, Hole C0018

Sample Number	Sample Name	Depth (mbsf)	% Sand	% Silt	% Clay		
1	C0018A-11H-1 W	90.11	5.35	56.31	38.33	Clayey Silt	
2	C0018A-12H-1 W	99.63	8.52	51.68	39.79	Clayey Silt	
3	C0018A-13H-1 W	108.87	7.42	56.48	36.11	Clayey Silt	
4	C0018A-14H-1 W	118.34	5.15	55.49	39.36	Clayey Silt	
5	C0018A-15H-2 W	127.56	32.89	48.65	18.45	Sandy Silt	
6	C0018A-15H-3 W	128.24	12.35	63.98	23.67	Clayey Silt	MTD-B
7	C0018A-15H-4 W	129.49	8.73	60.24	31.03	Clayey Silt	MTD-B
8	C0018A-15H-6 W	130.75	7.14	63.14	29.72	Clayey Silt	MTD-B
9	C0018A-15H-7 W	132.01	6.28	50.61	43.11	Clayey Silt	MTD-B
10	C0018A-15H-8 W	133.27	7.85	43.31	48.84	Silty Clay	MTD-B
11	C0018A-15H-9 W	134.53	7.85	56.21	35.94	Clayey Silt	MTD-B
12	C0018A-16H-1 W	136.62	16.13	50.32	33.55	Clayey Silt	MTD-B
13	C0018A-16H-2 W	138.02	6.43	60.82	32.75	Clayey Silt	MTD-B
14	C0018A-16H-3 W	139.53	9.84	74.83	15.33	Clayey Silt	MTD-B
15	C0018A-16H-4 W	140.70	7.89	59.41	32.70	Clayey Silt	MTD-B
16	C0018A-16H-11 W	143.00	2.88	40.79	56.33	Silty Clay	MTD-B
17	C0018A-17H-1 W	145.14	9.27	42.19	48.54	Silty Clay	MTD-B
18	C0018A-17H-2 W	146.42	4.05	65.72	30.22	Clayey Silt	MTD-B
19	C0018A-17H-3 W	147.74	6.01	74.26	19.74	Clayey Silt	MTD-B
20	C0018A-17H-4 W	149.06	3.69	43.82	52.49	Silty Clay	MTD-B
21	C0018A-17H-7 W	151.23	2.54	55.55	41.91	Clayey Silt	MTD-B
22	C0018A-17H-8 W	152.57	3.99	39.36	56.65	Silty Clay	MTD-B
23	C0018A-18H-1 W	154.16	6.28	36.55	57.17	Silty Clay	MTD-B
24	C0018A-18H-3 W	156.73	5.72	65.53	28.76	Clayey Silt	MTD-B
25	C0018A-19H-1 W	160.09	4.10	52.74	43.15	Clayey Silt	MTD-B
26	C0018A-19H-2 W	161.23	3.53	61.74	34.73	Clayey Silt	MTD-B
27	C0018A-19H-3 W	162.27	3.39	74.39	22.22	Clayey Silt	MTD-B
28	C0018A-19H-5 W	163.19	6.52	70.11	23.37	Clayey Silt	MTD-B
29	C0018A-20H-1 W	164.92	10.36	79.78	9.86	Silt	MTD-B
30	C0018A-20H-3 W	166.70	4.83	75.18	19.99	Silt	MTD-B
31	C0018A-20H-4 W	168.03	1.86	54.96	43.18	Clayey Silt	MTD-B
32	C0018A-20H-6 W	169.40	1.63	50.66	47.71	Clayey Silt	MTD-B
33	C0018A-20H-7 W	170.78	3.28	55.13	41.59	Clayey Silt	MTD-B
34	C0018A-20H-8 W	172.17	9.74	68.14	22.11	Clayey Silt	MTD-B
35	C0018A-20H-9 W	173.51	4.26	78.51	17.23	Silt	MTD-B
36	C0018A-21H-2 W	175.95	1.91	57.38	40.71	Clayey Silt	MTD-B
37	C0018A-21H-5 W	177.56	8.38	49.48	42.15	Clayey Silt	MTD-B
38	C0018A-22H-1 W	178.56	5.75	71.16	23.09	Clayey Silt	MTD-B
39	C0018A-22H-3 W	180.27	8.25	78.90	12.84	Clayey Silt	MTD-B
40	C0018A-22H-4 W	180.97	3.07	55.25	41.68	Clayey Silt	MTD-B
41	C0018A-22H-8 W	183.38	4.09	69.05	26.85	Clayey Silt	MTD-B
42	C0018A-22H-9 W	184.34	5.04	72.64	22.31	Clayey Silt	MTD-B
43	C0018A-22H-10 W	185.33	4.64	64.37	30.99	Clayey Silt	MTD-B
44	C0018A-22H-11 W	185.98	4.09	61.38	34.53	Clayey Silt	MTD-B
45	C0018A-22H-12 W	186.98	4.71	65.27	30.01	Clayey Silt	MTD-B
46	C0018A-23H-1 W	188.42	5.07	67.40	27.53	Clayey Silt	MTD-B
47	C0018A-23H-1 W	188.62	3.86	68.74	27.40	Clayey Silt	MTD-B
48	C0018A-23H-2 W	189.07	54.78	32.56	12.66	Silty Sand	
49	C0018A-23H-3 W	190.09	42.65	37.85	19.50	Silty Sand	
50	C0018A-24T-1 W	191.17	59.39	38.58	2.03	Silty Sand	